

Efficient Magic State Factory Via Transversal Non-Clifford Gate

I-Chi Chen,^{1,*} Hrushikesh Pramod Patil,^{2,†} Huiyang Zhou,² and Andrew Sornborger¹

¹*Los Alamos National Laboratory, Computing and Artificial Intelligence Division, Los Alamos, NM, USA*

²*Department of Electrical and Computer Engineering,
North Carolina State University, Raleigh, NC, USA*

(Dated: June 16, 2026)

Magic-state preparation is a central component of fault-tolerant quantum computing. Recent theoretical and experimental successes in code-switch-based magic-state preparation have underscored the promise of these methods for quantum error correction. Similarly, magic-state cultivation has likewise been demonstrated in both numerical and experimental settings. However, a thorough comparison between magic-state cultivation and code-switch-based magic-state factories is still missing. In this work, we carry out end-to-end simulations of magic-state preparation using code switching and compare its resource requirements and performance against magic-state cultivation. As part of this analysis, we develop a lattice-surgery protocol for transfer between the doubled color code and the rotated surface code. We extend the complete code-switching protocol to the $d = 5$ doubled color code and perform the corresponding end-to-end simulations. Finally, we propose two fault-tolerant magic-state preparation protocols that combine phase-kickback checks with a transversal non-Clifford gate.

I. INTRODUCTION

The realization of a universal fault-tolerant quantum computer (FTQC) [1–3], which could provide exponential speed-ups for some algorithms relative to a classical computer, has become the focus of quantum information science. Quantum error correction (QEC) codes have been touted as the way to achieve FTQC. An important component for QEC codes is a transversal gate set. Transversal gates act independently across corresponding physical qubits in logical code blocks to create a corresponding logical operation without error. Transversal gate sets greatly reduce the complexity of implementing fault-tolerant operations, which is pivotal to the practical implementation of fault-tolerant computations.

Unfortunately, there is no free lunch when it comes to a fully transversal and universal fault-tolerant gate set. According to the Eastin-Knill theorem [4], no single quantum error code has a complete universal gate set that can be implemented transversally. Generally, for specific codes, Clifford gates can be implemented using lattice surgery (LS) [5, 6] or transversal gates [7]. Non-Clifford gates, like the T gate, are required to complete a universal gate set but are generally not implemented transversally for the same codes. The most common way to implement a non-Clifford gate is to prepare a magic state (typically probabilistically) and teleport it into the arbitrary logical state as the logical operation. Alternatively methods, such as code switching (CS) [8] be-

tween QEC codes, can also be used to complete a universal gate set. In this context, one switches between a code supporting all transversal Clifford gates and another code that supports a transversal non-Clifford gate. With CS techniques, one can achieve the universal fault-tolerant gate set. An example is CS between the 2D color code and 3D color code or double color code, which has transversal Clifford gates [9–11] and transversal T gate (non-Clifford) [12], respectively. This approach to QEC has led to CS being studied extensively between codes that support the aforementioned criteria [13–18].

The fault-tolerant state preparation of a 3D color code state is complicated. Although the 2D color code has potentially better performance per physical qubit than its competitor, the rotated surface code, decoding on the 2D color code has proven to be difficult. Only the maximum likelihood [19], tesseract [20], and Vibe [21] decoders, which have longer runtime, allow color codes to beat the surface code in terms of the performance per physical qubit. Their long runtime makes the practical implementation of 2D color code infeasible. In contrast, surface codes with the minimum-weight perfect matching (MWPM) decoding can achieve good performance [22] with much lower runtime overhead. However, the initialization and accurate decoding of the 3D color code or doubled color code remains a challenge. This limits the potential for building a universal fault tolerant quantum computer solely based on CS between 2D color code and 3D color code.

Instead of directly constructing a universal quantum computer with just the 2D and 3D color codes, Ref. [23] directly uses these two codes as a magic state factory, which allows one to discard non-trivial syndrome mea-

* ichen@lanl.gov

† hpatil2@ncsu.edu

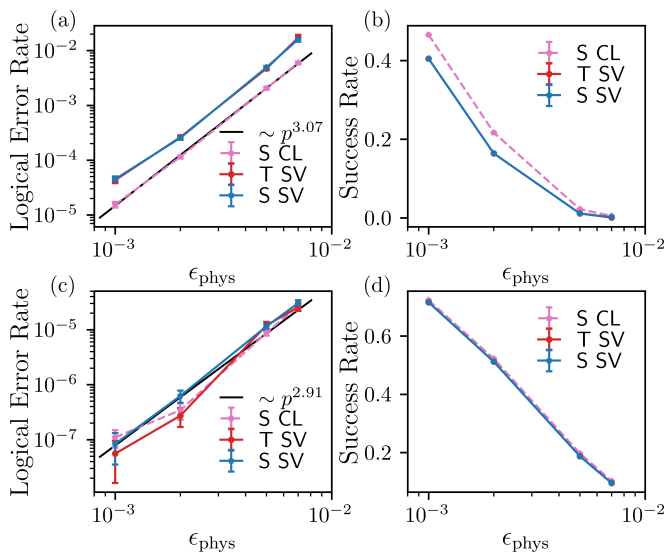


FIG. 1. **Performance of magic state preparation using transversal gate.** (a) The logical infidelity and (b) the success rate of $T|+\rangle_L$ and $S|+\rangle_L$ preparations using transversal T are estimated by state vector (SV) simulation (red line: $T|+\rangle_L$ and blue line: $T|+\rangle_L$) and Clifford (CL) gate simulation (purple line: $S|+\rangle_L$) with varying noise levels. Note that the Clifford circuit simulation is simulated under the uniform noise model, while the state vector simulation is executed under an approximate uniform noise model, which serves as an upper bound for the uniform noise model and can be simulated using fewer qubits. The exponents of fitting lines are calculated using `Scipy.state.linregress` function. Error bars correspond to the standard error of the mean.

surement outcomes [24]. The corresponding protocol has also been successfully implemented on trapped-ion quantum hardware [23]. However, extending the protocol to $d = 5$ is complicated because of its large qubit counts. In particular, fault-tolerantly preparing the $d = 5$ tetrahedral color code requires 65 qubits [25]. Alternatively, one can also use the $d = 5$ doubled color code using double construction with the 2D $d = 5$ color code. Nevertheless, fault-tolerant initialization of the doubled color code remains a challenge.

Magic State Distillation (MSD) [6, 26–28] is one of the popular and explored techniques to fault tolerantly prepare magic states. However, MSD’s huge space-time overhead is a bottleneck for near term implementation. Recently, magic state cultivation (MSC) [29] was developed to obtain a good enough magic state with a cost equivalent to performing a lattice surgery based CNOT on a surface code. Un-grown MSC has recently been experimentally demonstrated [30] on a superconducting platform. All MSC protocols transfer high-quality magic states to the surface code, which can be easily decoded using an MWPM decoder. $T|+\rangle_L$ cultivation on the color code can be achieved through code grafting [29] or lattice surgery onto the surface code [31]. Moreover, $T|+\rangle_L$ cultivation on SRP-3 (5) codes can be morphed

into an RP^2 code, a variant of the surface code [32]. In this context, the fold-transversal H_{XY} , which is composed of a transversal X gate and a fold-transversal S gate on the unrotated surface code, enables one to cultivate magic states on the surface code [33]. Since simulating non-Clifford gates on a classical computer is computationally expensive, most simulations rely on the assumption that the discrepancy between $T|+\rangle_L$ (non-Clifford) and $S|+\rangle_L$ (Clifford) cultivation does not vary with code distance or noise strength, thereby using $S|+\rangle_L$ cultivation as a proxy for $T|+\rangle_L$ cultivation. However, it is not clear that this assumption is warranted. For instance, recent simulations for un-grown MSC on the $d = 5$ color code show that $T|+\rangle_L$ cultivation infidelity is 8 times that of $S|+\rangle_L$ cultivation [34]. Moreover, a recent paper shows that the logical infidelity discrepancy between proxy state and real magic state cultivation becomes larger and larger as the noise strength decreases [35].

Although a comparison between MSC and CS protocols was made in Ref. [24], the authors ignore idling noise for the CS protocol. Moreover, the results do not include the end-to-end simulation. Here, we re-evaluate the performance of magic state preparation using a transversal non-Clifford gate and CS protocol under idling noise. Our protocol consists of three primary steps: first, we prepare a high-fidelity magic state on a small-distance QEC code utilizing a transversal non-Clifford gate. Second, we code-switch this state to an identical-distance 2D color code. Finally, the 2D color code is grown and escaped into a larger-sized surface code.

We also compare the performance of $T|+\rangle_L$ and $S|+\rangle_L$ ’s preparation using the CS protocol with and without idling noise. We discuss the code growing strategy and extend the protocol to code distance $d = 5$. To reduce space overhead, inspired by Ref. [31], we establish an LS protocol between a doubled color code and a rotated surface code of which we control the target size. Finally, we propose two protocols composed of a double-phase kickback, with MSC as one component, and a transversal non-Clifford gate to prepare the magic state with higher fidelity.

II. CODE SWITCH AND GROWING

Here, we study magic state preparation on the doubled color code which has transversal T gate. The doubled color code is particularly suitable for near-term devices with all-to-all connectivity and long lifetime physical qubits such as neutral atom [36] and trapped ion systems [23] due to their low idling error rates. To test the consistency of performance between $T|+\rangle_L$ and $S|+\rangle_L$ preparation, we simulate both states’ preparation under a uniform noise model with and without idling noise on a state vector simulator. To mitigate the effect of idling noise, we shorten the circuit depth for $|+\rangle_L$ preparation using the MQT QECC package [37, 38] and implement stabilizer measurement using Bell states. However, it is

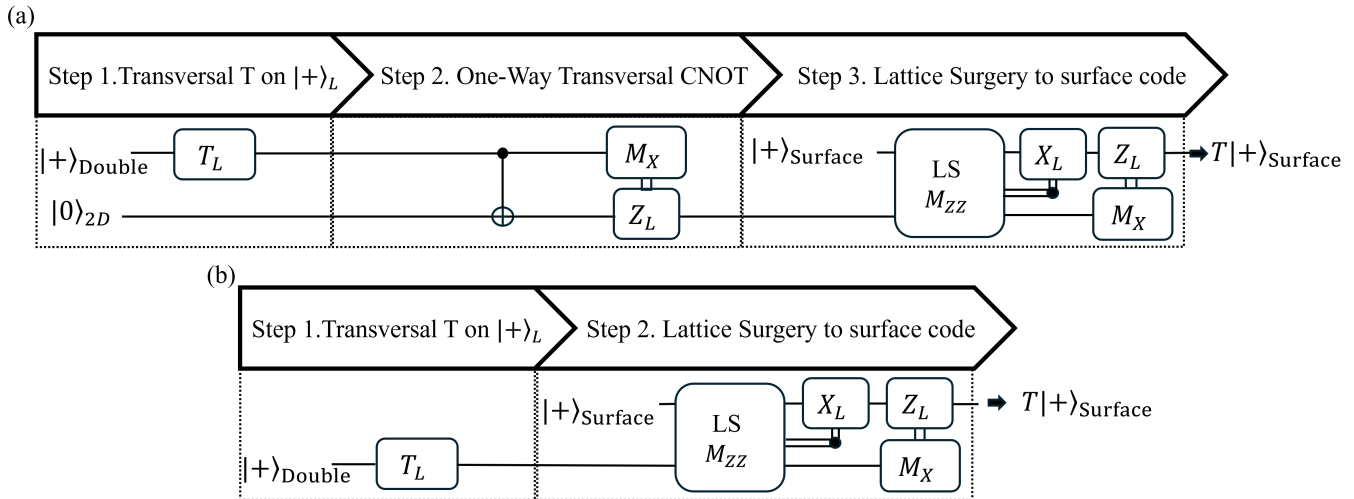


FIG. 2. **The workflow of the end-to-end process for preparing a magic state using the doubled color code.** The procedure of end-to-end magic state preparation using transversal gate and lattice surgery from (a) 2D color code and (b) double color code into a large rotated surface code is depicted. At the first step, before the transversal T gate (shown as T_L), one round of Z -type stabilizer measurements is applied. For the second step at (a), CS is applied from doubled color code to 2D color code using a one-way transversal $\overline{\text{CNOT}}$ gate. Then, the logical X is measured (represented by M_X). If the outcome gives 1_L , the logical Z will be applied to the 2D color code. Otherwise, no operation is implemented on the 2D color code. In the final step of (a) and (b), the color code is converted into a rotated surface code using lattice surgery (LS) that also measures the ZZ_L (shown as M_{ZZ}) of the surface and color codes. If the M_{ZZ} measurement gives a non-logical zero, X_L operations are applied to the surface code. Finally, the color code is measured in the X_L basis. If the measurement outcome is not logical zero, Z_L gates are implemented on the surface code.

computationally expensive to do a state vector simulation of this circuit, due to the large number of qubits (more than 32) involved. Thus, we approximate the corresponding noisy circuit (more details about the approximate noisy circuit in Appendix B) with a smaller, noisy circuit.

In Fig. 1, we observe that both state preparations using transversal gates have consistent performance between the $S|+\rangle_L$ and the $T|+\rangle_L$ preparation on the $[[15,1,3]]$ tetrahedral code. In the upper panel of Fig. 1, although the Clifford circuit simulation under idling noise yields different results from the state vector simulation, the state vector simulation result shows the actual outcome when a magic state is prepared using the transversal gate. The logical error rate achieved is about 1.3×10^{-5} with a physical gate error rate of 10^{-3} , and corresponding success rate around 46%. The corresponding $S|+\rangle_L$ preparation's logical infidelity physical error rate exponent of roughly 3.07, which is close to the $[[15,1,3]]$ color code distance. Without idling noise, the result of the Clifford simulation matches that of the state vector simulation. The corresponding infidelity can be below 10^{-7} , with a success rate of about 65 percent, when the physical gates' noise is around 10^{-3} . Based on the consistency of $S|+\rangle_L$ and $T|+\rangle_L$'s logical infidelity from the approximate noisy circuit, we believe that $T|+\rangle_L$ preparation on $[[15,1,3]]$ code has a similar performance as $S|+\rangle_L$'s even in the state vector simulation.

Although it is hard to expand this doubled color code

into a color code with a higher code distance, one can alternatively employ a CS protocol for magic state preparation. The CS protocol [24] for magic state preparation shares the same fundamental ideas as magic state cultivation: preparing a high-fidelity magic state on a small code with full postselection and then immediately grow the code into a surface code with a larger code distance. In Fig. 2(a), we depict the protocol:

1. Prepare the magic state in the 3D color code by applying the transversal T gate on $|+\rangle_L$ state. Before the transversal T gate, Z -type stabilizers are measured for postselection.
2. Use the transversal $\overline{\text{CNOT}}$ -based CS proposed in Ref. [17] to teleport the state into the 2D color code, which initially is prepared in the state $|0\rangle_L$.
3. Grow the color code into a grafted surface code proposed by the Google team [29] or into a rotated surface code via lattice surgery [31].

This method requires a step to code switch the 3D color code to the 2D color code. Alternatively, in step 2, we directly convert the 3D color code into a rotated surface code via LS, shown in Fig. 2(b). Thus, the protocol becomes

1. Prepare the magic state in 3D color code by applying the transversal T gate on the $|+\rangle_L$ state. Before the transversal T gate, the Z -type stabilizers are measured for postselection.

- Directly expand the code into a larger rotated surface code via LS.

In the subsequent section, we will present examples of different code distance CS protocols and details on growing using LS.

A. $d = 2$ case

The smallest code that supports the transversal T gate is the $[[10,1,2]]$ Vasmer-Kubica code [39] (more details in Appendix). Although CS between a $[[10,1,2]]$ code and a $[[7,1,3]]$ code has been proposed and demonstrated on trapped-ion quantum hardware [18], the protocol requires additional stabilizer measurements, which are time-consuming, and therefore prone to errors. Alternatively, based on Ref. [17], one can teleport the state's information from $[[10,1,2]]$ code to $[[7,1,3]]$ code using a one-way transversal CNOT gate connecting the bottom face of the $[[10,1,2]]$ code to the $[[7,1,3]]$ code, thus avoiding stabilizer measurements. This is possible since the stabilizer group and the logical Pauli operators of the two codes remain invariant after the transversal $\overline{\text{CNOT}}$ gate

$$\overline{\text{CNOT}}\bar{X}_{[[10,1,2]]}\overline{\text{CNOT}} = \bar{X}_{[[10,1,2]]}\bar{X}_{[[7,1,3]]} \quad (2.1)$$

$$\overline{\text{CNOT}}\bar{Z}_{[[7,1,3]]}\overline{\text{CNOT}} = \bar{Z}_{[[10,1,2]]}\bar{Z}_{[[7,1,3]]} \quad (2.2)$$

where $\bar{X}_{[[10,1,2]]}$ ($\bar{X}_{[[7,1,3]]}$) and $\bar{Z}_{[[10,1,2]]}$ ($\bar{Z}_{[[7,1,3]]}$) are respectively X and Z logical operators for the $[[10,1,2]]$ ($[[7,1,3]]$) code. Thus, one can also apply the CS protocol to prepare $T|+\rangle_L$ on a 2D color code.

After CS to the $d = 3$ Steane code, one also measures the Vasmer-Kubica code in the X_L basis to determine whether the logical Z operator is applied to the Steane code or not. The logical X operator of the Vasmer-Kubica code is

$$X_L = X_1X_2X_3X_4X_5X_6X_7 \quad (2.3)$$

where the subscript labels of X correspond to the position shown in Fig. 12(a) in the Appendix. Hence, only 7 qubits at the bottom are measured in the X basis for X_L measurement results. However, one can still measure all 10 qubits to obtain other X -stabilizer results. If any stabilizer outcomes give a non-trivial syndrome, one discards the corresponding shot. However, the Z type error's code distance is only 2. Although the code can be switched to a $d = 3$ 2D color code, the 2-weight Z type errors will dominate the logical error. Hence, we focus on higher distance codes instead.

B. $d = 3$ case

For $d = 3$, the 3D color code switch to the $d = 3$ Steane code via transversal $\overline{\text{CNOT}}$ gate has been demonstrated in Ref. [24]. Although one can measure all stabilizers

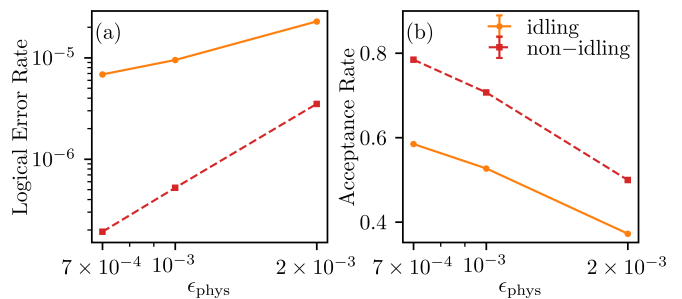


FIG. 3. **The performance for ungrown $d = 3$ code switch protocol (with and without the idling noise).** (a) The logical error rates and (b) the acceptance rates varying with the physical noise strength for $[[15, 1, 3]]$ (with idling noise in orange ('+' markers) and with idling noise labeled in red dashed lines ('x' marker).) CS protocol. The number of rounds is $r = 2$ after the transversal CNOT code switch. The error bar is the standard error from the successful shots (errors bars are not visible in the plot as the errors bars are order of magnitude smaller than the values of logical errors and acceptance rate).

with only four extra ancilla qubits using the method in Ref. [24], unparallelized stabilizer measurements under idling noise end up inducing more logical error. Here, inspired by Ref. [40], we implement a faster stabilizer measurement using Bell pairs to measure all Z (X)-type stabilizers in parallel. For the $[[15, 1, 3]]$ code, a total of 20 extra qubits are required to measure all 10 Z stabilizers. Measuring 4 X stabilizers requires a total of 8 extra qubits. After CS, we also use Bell pairs to optimize the parallelization of the Steane code's syndrome measurement. The Bell pairs help us obtain Z stabilizer measurement outcomes with a circuit depth of 8. Moreover, in order to optimize the performance of $[[15, 1, 3]]$ code preparation in $|+\rangle_L$, we implement the MQT QECC package [37, 38], which allows us to prepare the $|+\rangle_L$ with circuit depth 5 and an extra 8 flag qubits to verify the tetrahedral code $|+\rangle_L$. In total, the space-time volume, which is defined as the number of active qubits times the circuit depth, for initializing $|+\rangle_L$ is 214 (more details in the Appendix). For the initialization of the $d = 3$ Steane code, we implement the same $|+\rangle_L$ preparation method as Ref. [36], which prepares $|0\rangle_L$ on the $d = 3$ Steane code with circuit depth 4, using 2 flag qubits to check the quality of $|+\rangle_L$. For the entire $d = 3$ CS, the total space-time volume is 615; around 50 percent less than that in Ref. [24] (more details in Appendix).

To test its performance, we also simulate the CS under uniform noise models with and without idling noise. However, simulating $T|+\rangle_L$ preparation between $d = 3$ Steane code and 3D color code involves at least 22 data qubits, which does not include the ancilla qubits for syndrome measurement. The corresponding state vector simulation with at least 10^8 shots is complicated. Thus, similarly to Ref. [29], we simulate $S|+\rangle_L$ preparation using Clifford circuit simulation instead. To evaluate the logical infidelity of the magic state $S|+\rangle_L$ prepared using

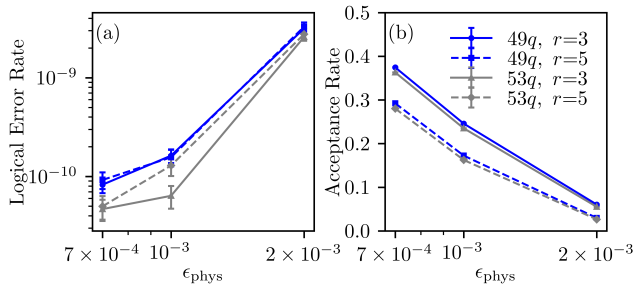


FIG. 4. **The performance for ungrown $d = 5$ code switch protocol (without idling noise).** (a) The logical error rates and (b) the acceptance rates varying with the physical noise strength for $[[49, 1, 5]]$ ($49q$ in blue lines) and $[[53, 1, 5]]$ ($53q$ in green lines) CS protocol. The dashed and solid lines mean different number of syndrome measurement rounds ($r = 5$ and $r = 3$ respectively) after the transversal CNOT code switch. The error bar is the standard error from the successful shots.

CS, we add one extra ideal syndrome measurement after a few rounds of noisy measurements in order to filter out all of the residual errors. We also apply the ideal logical S^\dagger gate after the ideal syndrome measurement. We measure the entire 2D color code’s data qubits in the X basis. We calculate the corresponding logical error rate as the number of 1_L results divided by the total number of successful shots that yield all-zero syndrome measurements.

In Fig. 3, the performance of $d = 3$ CS is visualized. With idling noise, the logical error rates are around 10^{-5} when physical gates’ error rates range from 2×10^{-3} to 7×10^{-4} . Compared to the performance of ungrown $T|+\rangle_L$ cultivation in $d = 3$ Steane code [29], the performance of $d = 3$ CS is around 10 times worse than MSC. On the other hand, the success rates are around 55% – 60%, which is close to the success rate of ungrown MSC. Without idling noise, when physical gates’ error rate is at 10^{-3} , the logical error rate is about 5×10^{-7} , which is close to the result from Ref. [24]. However, since we implement an extra three rounds of syndrome measurement after CS, the success rate is 70%, which is lower than the 84% of Ref. [24].

C. $d = 5$ case

To extend the doubled color code from $d = 3$ to $d = 5$, one can construct the 3D $d = 5$ color code using a doubling transformation from the $d = 5$ 2D color code [41, 42]. If one chooses a $d = 5$ (4, 8, 8) 2D color code $[[17, 1, 5]]$, after the doubling construction, the 3D color code becomes a $[[49, 1, 5]]$ code. On the other hand, if the chosen code is the (6, 6, 6) 2D color code $[[19, 1, 5]]$, the corresponding 3D color code is $[[53, 1, 5]]$ using the doubling construction. The constructed 3D color codes $[[49, 1, 5]]$ ($[[53, 1, 5]]$) also support the transversal CNOT

CS with the $[[17, 1, 5]]$ ($[[19, 1, 5]]$) Steane code [43]. These 3D color codes can be visualized as recursively stacked color codes [44, 45]. As Fig. 13 shows, the corresponding code resembles a qubit on top of stacks of paired layers of $d = 3$ 2D color codes and paired layers of $d = 5$ 2D color codes. Moreover, the tetrahedral color code can be extended from $d = 3$ to $d = 5$ [25]. However, the corresponding $d = 5$ tetrahedral color code requires more physical qubits for encoding (65 qubits for $d = 5$). Thus, we only focus on the recursively stacked color code for that case.

In order to fault-tolerantly prepare $|+\rangle_L$ and $|0\rangle_L$ for double and 2D color codes, respectively, we employ the MQT QECC package [37, 38] with extra flag qubits [46] to check whether the prepared state is correct or not. Before the end-to-end CS-based magic state preparation, we simulate ungrown magic state preparation to understand how many rounds of syndrome measurements are required after CS. However, the simulation of $T|+\rangle_L$ preparation using a transversal T gate is beyond the Clifford simulation as the T gate is non-Clifford. Thus, we simulate $S|+\rangle_L$ proxy state preparation instead and estimate the performance of the $T|+\rangle_L$ preparation based on the $d = 3$ state vector simulation result. Moreover, since the $d = 5$ double color code has 35 Z stabilizers for $[[49, 1, 5]]$ code (38 Z stabilizers for $[[53, 1, 5]]$ code), with idling noise, the corresponding success rate to get all zero syndrome measurements is very low. Hence, we only simulate $d = 5$ CS under uniform noise without the idling noise.

In Fig. 4(a), the logical error rates of the preparation of the magic state using CS are around $10^{-11} - 10^{-9}$ with noise strengths in the range $7 \times 10^{-4} - 2 \times 10^{-3}$. Two extra rounds of syndrome measurement do not improve infidelity. Instead, as Fig. 4(b) shows, the corresponding success rates are about 20 percent less than those with fewer rounds of syndrome measurement. Overall, the success rate for both codes is about 10% – 40% when the physical error rate is around $2 \times 10^{-3} - 7 \times 10^{-4}$. While $[[53, 1, 5]]$ slightly outperforms $[[49, 1, 5]]$ in terms of infidelity, $[[49, 1, 5]]$ ’s CS has a higher success rate than $[[53, 1, 5]]$ ’s.

D. Code Growing

To maintain low logical errors and perform error correction on the code, it is necessary to expand the small code into a larger code immediately. However, directly expanding the color code into a larger color code introduces too many logical errors due to the Chromobius decoder’s poor performance [29, 47]. Alternatively, one can expand the color code into a code that can be decoded with minimum weight perfect matching (MWPM) decoder [22]. One can expand the color code using grafting techniques into a surface code. Another way is to switch the 2D color code to a larger surface code via lattice surgery. Here, we not only implement LS from

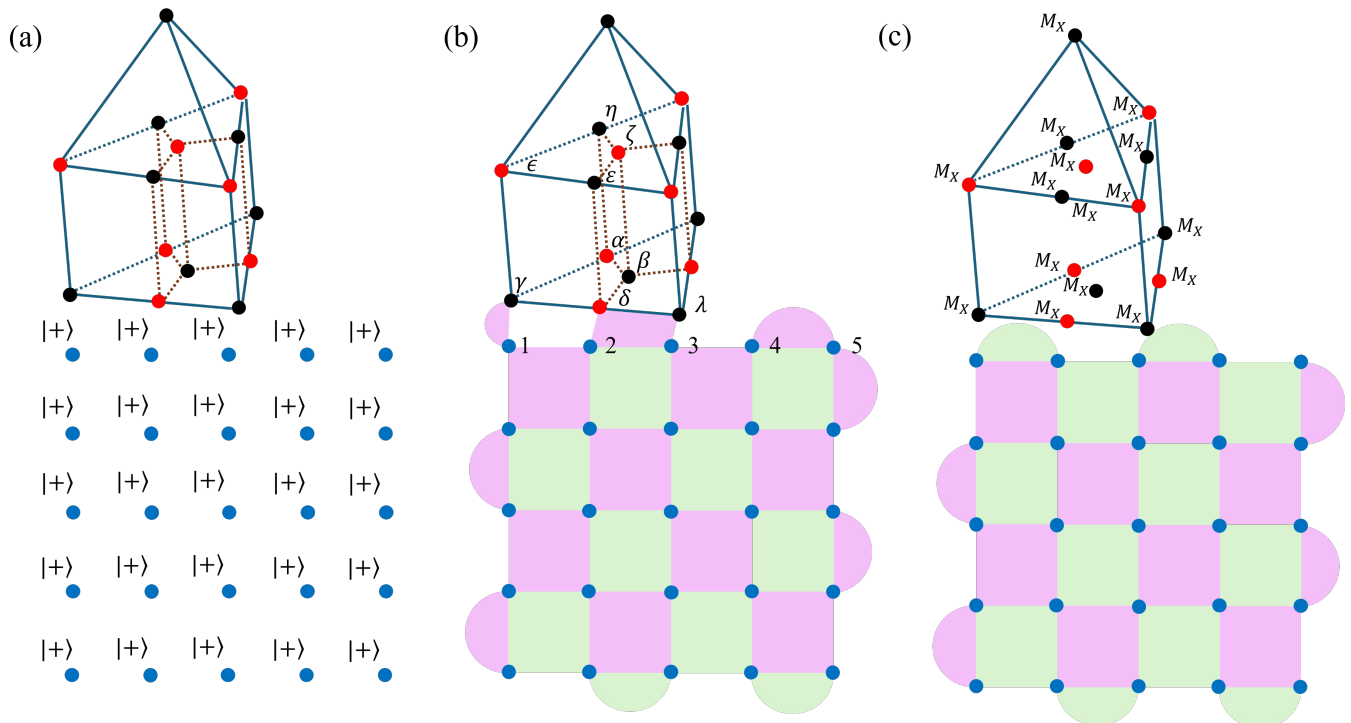


FIG. 5. **The illustration of lattice surgery between 3D color code and rotated surface code.** (a) The surface code initialized with all data qubits $|+\rangle$ states and the color code with $T|+\rangle_L$. (b) The X-type (green) and Z-type (pink) stabilizers from the surface code and the boundary between surface code and color code. (c) The stabilizers of the surface code after the lattice surgery and X_L measurement of the color code. Since the stabilizer $X_\alpha X_\beta X_\gamma X_\delta X_\epsilon X_\zeta X_\eta$ from color code doesn't commute with $Z_\gamma Z_1$ and $Z_\delta Z_\lambda Z_2 Z_3$, the stabilizer becomes $X_1 X_2 X_\alpha X_\beta X_\gamma X_\delta X_\epsilon X_\zeta X_\eta$ during the lattice surgery. After the lattice surgery, the color code is measured in the X_L basis by measuring all qubits individually in X basis (shown as M_X). If there are odd number of 1s result, the logical outcome is 1_L ; otherwise, the logical outcome is 0_L .

the 2D color code to the surface but also develop an LS protocol to transform a doubled color code into a larger surface. After the LS, one needs to apply several rounds of syndrome measurement and simultaneously wait for the decoding result from the decoder. Based on the complementary gap's result calculated from the decoder [48], one can set up a threshold to discard corrupted results and get a higher quality magic state.

One of the issues for LS between a 2D color code and the surface code is the parallelization of the color code and the surface code's stabilizer measurements. The circuit depth of Surface code's X-type and Z-type stabilizers measurement is shorter than those of the 2D color code using superdense cycle. In order to parallelize color code and surface code's syndrome extraction, differently than Ref. [31], we implement syndrome measurement using a standard color code cycle with Bell flagging. The X(Z)-type stabilizer measurement of the color code roughly matches one round of the surface code cycle. Hence, for $d = 3$ case, there are three rounds of surface code stabilizer measurement, while there are only two rounds for the 2D color code (including X stabilizer measurement at the final measurement to get a logical X result) during LS. The stabilizers at the boundary between 2D color code and the rotated surface code are measured 3 times.

Moreover, instead of switching to an intermediate-sized rotated surface code, we directly perform LS to the 2D color code with the surface code at the targeted size.

The procedure of 3D color code switching into the rotated surface code via LS is very similar to that from 2D color code. The only difference is that the syndrome measurement of the 3D color code is more complex than that of the 2D color code, whose corresponding stabilizers can be measured using a superdense cycle or a standard color code cycle. Inspired by Ref. [40], using an extra flag qubit paired with a readout qubit as a Bell pair for each stabilizer measurement (in total, 20 ancilla qubits are required), we can parallelize all 10 Z stabilizer measurements for the $[[15,1,3]]$ code. Similarly, for 8-weight X stabilizers, we also perform each stabilizer measurement with a Bell pair. We also parallelize all 4 X stabilizer measurements. Thus, we can also apply LS between the $d = 3$ 3D color code and the rotated surface code. The corresponding LS procedure, shown as Fig. 5, is as follows:

1. The data qubits on the rotated surface are all initialized as $|+\rangle$ after the preparation of $T|+\rangle_L$ on the 3D color code.
2. The surface code's stabilizers shown in Fig. 5(b)

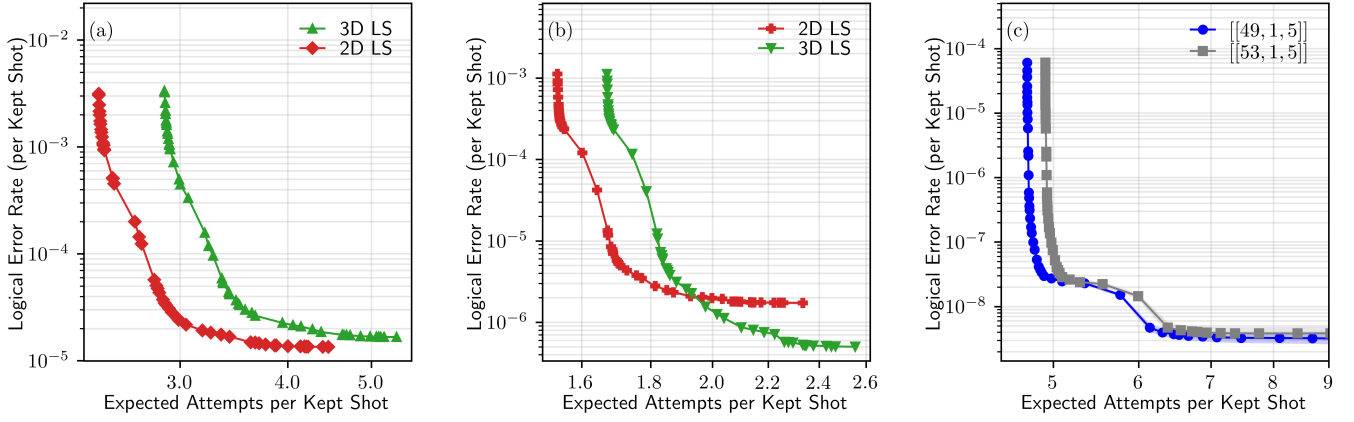


FIG. 6. **End-to-end simulation results for magic state preparation using a transversal non-Clifford gate.** The logical infidelity of simulation for (a) $d = 3$ with idling noise, (b) $d = 3$ without idling noise, and (c) $d = 5$ without idling noise. The curves vary with complementary gap threshold to postselect the shot with logical error-prone syndrome. In the $d = 3$ cases, 3D LS (2D LS) means that the end-to-end simulation including the lattice surgery from doubled (2D) color code to rotated surface code ($d_f = 11$). For $d = 5$ case, $[[49, 1, 5]]$ ($[[53, 1, 5]]$) represents the end-to-end simulation including the code switching from $[[49, 1, 5]]$ ($[[53, 1, 5]]$) code to $[[17, 1, 5]]$ ($[[19, 1, 5]]$) code and lattice surgery from 2D color code to rotated surface code ($d_f = 11$). The shaded areas indicate standard sampling error.

are measured three times. Meanwhile, X or Z stabilizers of the 3D color code are measured. At even-numbered cycles of the surface code syndrome measurement, the X stabilizers of the color code are measured except for $X_\alpha X_\beta X_\gamma X_\delta X_\epsilon X_\zeta X_\eta$ and $X_1 X_2 X_\gamma X_\delta$ stabilizers since it becomes $X_1 X_2 X_\alpha X_\beta X_\gamma X_\delta X_\epsilon X_\zeta X_\eta$ after the first round of syndrome measurement. Otherwise, Z stabilizer measurements are implemented. In addition, the Z stabilizers, $Z_\gamma Z_1$, $Z_\delta Z_\lambda Z_2 Z_3$, and $Z_4 Z_5$, at the boundary between the color code and the surface code are also measured in every surface code cycle. The results of these stabilizers give us the $Z Z_L$ result which determines whether the X_L operator is applied after LS.

3. All data qubits on the 3D color code are measured in the X basis. The measurement of the color code's X stabilizers including $X_1 X_2 X_\alpha X_\beta X_\gamma X_\delta X_\epsilon X_\zeta X_\eta$ can also be obtained at the same time. If a measurement gives a non-trivial syndrome outcome, the result is discarded. The X_L measurement is determined by the parity of the total measurement. If it is even, $X_L = 0_L$; otherwise, $X_L = 1_L$. This also determines whether the Z_L operator is implemented.

After LS, in order to decode using a correlated MWPM decoder [22, 48], we discard shots with non-trivial syndromes from the color code or the boundary between the color code and the surface code. Moreover, similarly to Ref. [40], we use a noise model without noise triggering the stabilizer syndrome for the MWPM.

III. END-TO-END SIMULATION

Here, to evaluate the entire CS protocol's performance, we execute end-to-end simulation of the CS protocols. Since simulation beyond the Clifford circuit is expensive, we simulate $S|+\rangle_L$ in place of $T|+\rangle_L$ for the CS protocol. Due to the consistency between $S|+\rangle_L$ and $T|+\rangle_L$ preparation (the result shown in Fig. 1), the result of $S|+\rangle_L$ preparation should be close to that of $T|+\rangle_L$. We additionally assume that the complementary gap computation takes 10 rounds of surface code stabilizer measurement. After 10 rounds, we discard corrupted outcomes based on whether the corresponding gap passes the threshold. Since stabilizer measurement on the $d = 5$ doubled color code washes out too many shots, we do not simulate 3D LS from $d = 5$ doubled color code to surface code.

In Fig. 6, end-to-end simulations for $d = 3$ and $d = 5$ are visualized. The leftmost data point of each curve represents the logical error rate without complementary-gap-based soft postselection. The higher threshold cutoff on the complementary gap makes the corresponding logical error rates lower until the logical error (roughly) converges to a bound, which is the lowest logical error rate when using complementary-gap-based postselection. As Fig. 6(a) shows, with idling noise, the 2D LS and CS protocol requires fewer attempts per retained shot than 3D LS to reach its best logical fidelity, around 10^{-5} . Moreover, the logical infidelity of 3D LS is around 2×10^{-5} , which is similar to the logical error rate of 2D LS. Without idling noise (shown in Fig. 6(b)), the infidelity of 2D LS can reach below 2×10^{-6} with only 2 attempts per retained shot. On the other hand, the logical error using 3D LS can reach below 5×10^{-7} , but it requires 2.4

attempts per shot.

Without idling noise, the 2D and 3D LS results above imply that the initialization of the 2D color code and the transversal CNOT between two QEC codes induce extra logical errors. Thus, the 3D LS procedure outperforms that of the 2D LS in terms of infidelity. However, when idling noise is involved, the 3D LS procedure has a slightly worse outcome than that of 2D LS. In the $d = 5$ case shown in Fig. 6(c), CS from $[[49, 1, 5]]$ outperforms that from $[[53, 1, 5]]$ in terms of success rate and logical fidelity. For the $[[53, 1, 5]]$ CS, the logical infidelity can achieve 4×10^{-9} with a success rate of around 13.9 percent. In contrast, for the $[[49, 1, 5]]$ CS, the logical error rate can attain 3×10^{-9} with a similar success rate.

In addition to end-to-end performance, we also estimated the expected space-time volume per successful shot for the entire magic state preparation process, defined as

$$V = \frac{1}{f_M} \sum_i^M f_i V_i \quad (3.1)$$

with f_i and V_i the success rate and spacetime volume for i th part of the circuit (resp.). f_M is the total success rate of the entire circuit. The corresponding V s are estimated in table I. In the $d = 3$ case, with idling noise, the 2D LS V is 26.5% lower than 3D LS with the same final logical error rate, 1.5×10^{-5} . Compared to the MSC's V (around 50,000) on the color code [29, 33], the 2D LS V is lower, but MSC gives a higher fidelity magic state (2×10^{-6}). On the other hand, without idling noise, although V of 3D LS is still higher than 2D LS, the corresponding final logical error rate of 3D LS can reach 6×10^{-7} . In contrast, the logical error rate of 2D LS can only approach 2×10^{-6} . In the $d = 5$ case, since we do not parallelize the circuit well, the corresponding space volume of end-to-end is very large. We leave the optimization of the spacetime volume for $d = 5$ to the future work.

	V	Final logical error rate
2D LS w/ i.d. noise	39655	1.5×10^{-5}
2D LS w/o i.d. noise	29115	2×10^{-6}
3D LS w/ i.d. noise	53989	1.5×10^{-5}
3D LS w/o i.d. noise	34209	6×10^{-7}

TABLE I. **The expected spacetime volume per successful shot.** The expected spacetime volume per successful shot to achieve a given logical error rate after complementary-gap-based postselection for 2D and 3D lattice surgery (LS) with and without idling (i.d.) noise. More details about expected spacetime volume may be found in Appendix C.

IV. COMBINATION OF CULTIVATION AND TRANSVERSAL NON-CLIFFORD GATE

Although magic state preparation with transversal non-Clifford gates provides another way to prepare high

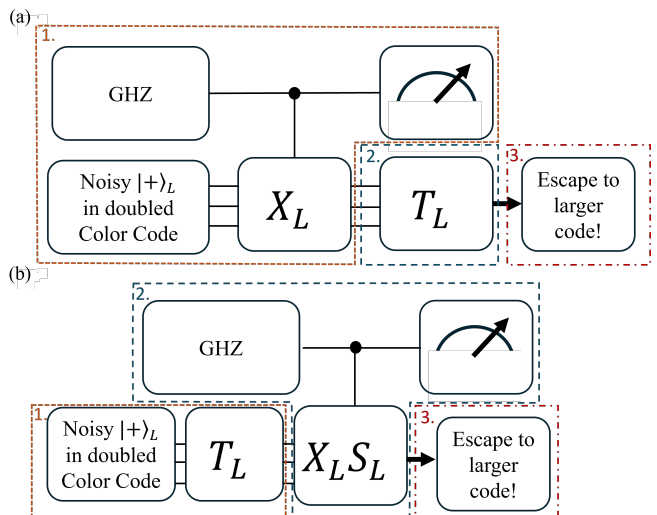


FIG. 7. **Illustration of a circuit composed of magic state cultivation and transversal non-Clifford gate.** In the first step, a noisy $|+\rangle_L$ state is prepared. Phase kickback measurement is used to check the quality of $|+\rangle_L$. One disentangles the GHZ state into a product state in the Z basis after the transversal CNOT (represented by control X_L in the figure). If the measurement outcome gives a non-zero result, it indicates that a non-trivial error has occurred in the code. One then directly abandons the shot. After the phase kickback measurement, the second step is to apply the transversal T gate (shown as T_L in the figure) to the 3D color code. Finally, the double color codes are converted into a large code. One can switch double color code into 2D color code via a transversal CNOT and transform it into a rotated surface code using lattice surgery. Alternatively, one can directly switch 3D color code into surface code using lattice surgery.

fidelity magic states, fault-tolerant preparation of 3D codes as $|+\rangle_L$ is challenging, especially for larger codes. Although one can use extra flag qubits to filter out bad logical state preparation, how to implement this is complicated. To address this issue, we propose a new method composed of MSC and code-switching protocols.

As Fig. 7(a) shows, our new protocol for preparing the magic states is the following:

1. Directly prepare noisy $|+\rangle_L$ (without extra flag qubits) with one round of syndrome measurement then utilize the MSC double phase kickback measurement to check the quality of $|+\rangle_L$.
2. Apply transversal T gate on 3D color code.
3. Implement CS from 3D color code to 2D color code, and LS to a larger rotated surface code. Alternatively, directly perform LS to a larger rotated surface code from the 3D color code.

Here, based on the transversal T and S gate results shown in Fig. 1, we also assume that the logical noise induced from $T|+\rangle_L$ using this method is similar to or lower than that from $S|+\rangle_L$.

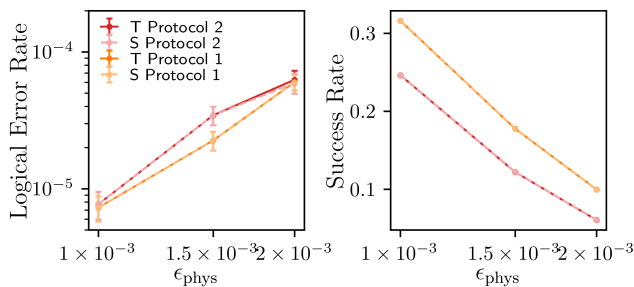


FIG. 8. **The statevector simulation for a combination of cultivation and transversal non-Clifford Gate.** (a) The logical infidelity and (b) the success rate of $T|+\rangle_L$ and $S|+\rangle_L$ preparation using both protocols, which include double phase check to check the quality of $|+\rangle_L$ and $T|+\rangle_L$ or $S|+\rangle_L$. The protocol 1 (2) represents the first (second) protocol, which has a phase kickback double check for $|+\rangle_L$ ($T|+\rangle_L$ or $S|+\rangle_L$). Here, we randomly choose seeds for the simulation, but T and S state's simulation share the same seed.

Another protocol combining MSC and transversal non-Clifford gates is to implement the transversal T gate first and apply the phase kickback check subsequently. In Fig. 7(b), the corresponding protocol is as follows

1. Prepare noisy $|+\rangle_L$ (without extra flag qubits) and apply transversal T after preparing the state. After the transversal T gate,
2. Implement double phase kickback measurement to check the quality of $T|+\rangle_L$.
3. Implement CS from 3D color code to 2D color code, and LS to a larger rotated surface code. Otherwise, directly perform LS to a larger rotated surface code from 3D color code.

Here, the double phase kickback check is similar to Ref. [33] and is composed of transversal X gate and S gate. In this case, one should apply extra physical T gates on the ancilla qubits to cancel the phase generated from $SXT|+\rangle_L = e^{i\frac{\pi}{4}}T|+\rangle_L$. According to Ref. [49], one can apply the T or T^\dagger gates on the auxiliary GHZ state after control XS^\dagger or XS . In total, for $d = 3$ doubled color code, a 15-qubit GHZ state is required. Alternatively, control XS^\dagger and XS can be paired together to cancel the corresponding phase on the auxiliary GHZ state. One of the GHZ ancilla qubits receives only one XS control operation. After disentangling the ancilla GHZ state into a Pauli basis product state, T^\dagger is applied on the corresponding ancilla qubit. In this case, a 7-qubit GHZ state is required for the phase kickback check. Similarly, one can also implement 2 control XT^\dagger and 2 control XT gates with the same control qubits of GHZ state. Hence, a 4-qubit GHZ state is required.

To test the consistency in performance between the preparation $S|+\rangle_L$ and $T|+\rangle_L$ for these two protocols,

we implement a state vector simulation before the end-to-end simulation. We apply the same strategy as in the Sec. II state vector simulation to estimate the corresponding logical error rate. We choose the 4-qubit GHZ state for the state-vector simulation to avoid complicated computation. Furthermore, in order to fairly compare the two protocols, we assume that control XS (XS^\dagger) in the second protocol is a two-qubit gate with a following two-qubit depolarized noise.

In Fig. 8, the $T|+\rangle_L$ and $S|+\rangle_L$ preparation using both protocols are almost consistent with each other. Compared to the second protocol, the first protocol stands out for its greater logical fidelity and higher success rate. At a physical gate error rate of 10^{-3} , the logical infidelities of both protocols are below 10^{-5} , which is much lower than the original result with only a transversal T (S) gate (shown in Fig. 1). For the end-to-end simulation, we also only simulate $S|+\rangle_L$ for the logical infidelity estimation of both protocols. To optimize the logical infidelity, we use a 15-qubit GHZ state to implement the double-phase-kickback check. Moreover, we use uniform noise with a physical error rate 10^{-3} to study how the success rate and logical error rates vary with the complementary gap.

In Fig. 9, the first protocol with the double-kick-phase check for $|+\rangle_L$ has similar performance as the second protocol with double-kick-phase check for $S|+\rangle_L$. As the complementary gap increases, more and more shots with logical error-prone syndromes get removed. For both protocols, the corresponding logical error rates reach the saturated value, which is around 10^{-5} with roughly 8 attempts per retained shot. Since 3D LS does not require the preparation of Steane code and transversal CNOT, the corresponding logical error rates of both protocols are lower than 2D LS. Among these methods, the first protocol with 3D LS has a slightly better logical error rate than the second protocol. Although the logical infidelity has slightly better performance than the original results (2D and 3D LS with idling noise) from Fig. 6(a), the expected attempts per retained shot are much higher than the original results.

In Table II, the expected spacetime volumes per successful shot for different protocols are estimated. Overall, the first protocol has slightly less expected spacetime volume per successful shot relative to the second protocol, obtaining a logical error rate of 1.5×10^{-5} . Compared with the original 3D LS result in Table I, the first protocol and the second protocol with 3D LS have lower V , since the double phase kickback check can filter out more shots before LS expansion. On the other hand, V for the first and second protocols with LS does not outperform that of the original 2D LS.

V. CONCLUSIONS

In this paper, we adopt a $d = 3$ CS protocol for magic-state preparation in the idling noise model and compare

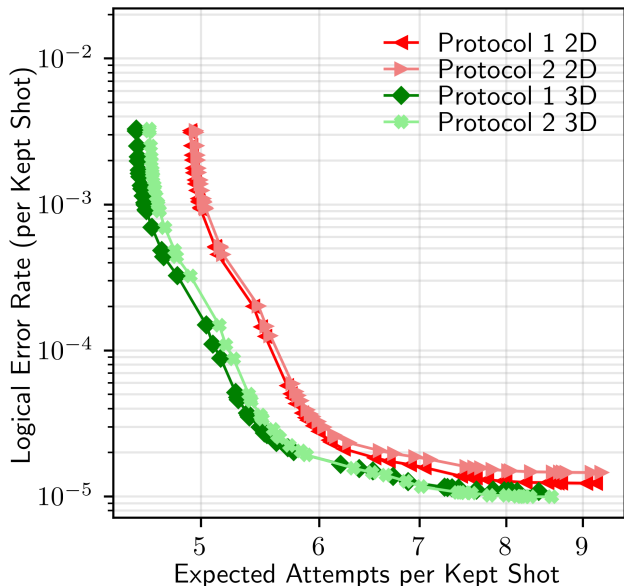


FIG. 9. **The end-to-end simulation for the combination of cultivation and transversal non-Clifford Gate.** The logical infidelity at physical error rate 10^{-3} varies with the attempts per kept shot, which is determined by the complementary gap-based postselection. The protocol 1 (2) refers to the first (second) protocol, which has the double phase kickback check to verify the quality of $|+\rangle_L$ ($S|+\rangle_L$). 2D (3D) means the different escape strategies using lattice surgery between Steane code (double color code) and rotated surface code.

	V	Final logical error rate
Protocol 1 3D LS	45443	1.5×10^{-5}
Protocol 2 3D LS	47181	1.5×10^{-5}
Protocol 1 2D LS	46170	1.5×10^{-5}
Protocol 2 2D LS	46733	1.5×10^{-5}

TABLE II. **The expected spacetime volume per successful shot for protocol 1 and 2** The expected spacetime volume per successful shot to achieve certain logical error rate after the complementary gap based postselection for combination of cultivation and transversal non-Clifford gate with 3D lattice surgery (LS) with idling noise. The more details about the expected spacetime volume are in appendix C.

with MSC. We observe that magic-state preparation using transversal non-Clifford gates shows strong consistency in performance between $S|+\rangle_L$ and $T|+\rangle_L$ preparations with and without idling noise. Although the state vector simulation result has large uncertainty in logical infidelity, it still shows that the CS protocol is a strong candidate for magic state preparation for near term devices, especially for all-to-all connectivity devices such as trapped-ion and neutral atom devices. Moreover, we provide the corresponding growth methodology to grow from the color code into the rotated surface code. In particular, inspired by Ref. [31], we establish a protocol

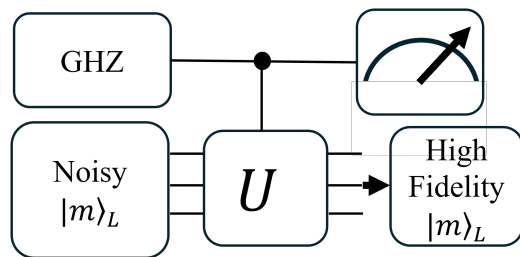


FIG. 10. **The phase kickback measurement for arbitrary $|m\rangle_L$.** The N qubits GHZ state $|\psi\rangle = \frac{1}{\sqrt{2}}(|0\rangle^{\otimes N} + |1\rangle^{\otimes N})$ are prepared to check the quality of $|m\rangle_L$ by applying transversally control U gates with target qubits which are the data qubits from the code state and the control qubits which are the qubit of GHZ state. For the final measurement, one can directly measure all ancilla qubits on X basis and check GHZ state's parity. If the final measurement outcome on GHZ state gives an odd parity result, indicating wrong logical state $|m\rangle_L$ preparation, one can discard the result. On the other hand, an even parity result means the high fidelity logical state $|m\rangle_L$ preparation. Alternatively, one can unentangle GHZ state back into all Z product state and measure all qubits in Z basis. If there are any non-zero results, it means the state is corrupted by noise. One can directly abandon the shot.

for LS between the doubled color code and the rotated surface code to reduce overhead. Additionally, we extend $d = 3$ CS based magic state preparation to $d = 5$. We show that without idling noise, the infidelity of the $d = 5$ CS based preparation for $S|+\rangle_L$ can reach 3×10^{-9} .

Finally, we also study the combination of a non-Clifford transversal gate and a double phase kickback check, a component of MSC. There are two ways to combine these two components together: (1) one using a double kickback phase check for $|+\rangle_L$ and then applying the transversal non-Clifford gate to prepare the magic state. And (2) applying the transversal non-Clifford gate first and implementing the double phase kickback check for $T|+\rangle_L$. Compared to the original CS protocol with only transversal T gate, the infidelity of the first protocol with the double kickback phase check is improved by 10%. In contrast, the second protocol cannot improve performance relative to the original CS protocol.

This work provides a more comprehensive numerical simulation of magic state preparation using transversal non-Clifford gates, including growth into larger surface code and the $d = 5$. simulation. The result shows that magic state preparation using transversal non-Clifford gates is another near-term device friendly option, especially for neutral atom and trapped-ion devices. Moreover, the corresponding method can be adopted into some magic state preparation methods such as unfolded distillation [50] and low overhead distillation in the color code [51]. Furthermore, an adapter can also be constructed that connects a 2D color code with a quantum low density parity check (qLDPC) code and surface code to teleport the magic state from the 2D color code to the

qLDPC code [52].

ACKNOWLEDGMENTS

We acknowledge valuable discussions with Chen Zhao, Pei-Kai Tsai, and Kaavya Sahay. This work was supported by the NNSA ASC Beyond Moore’s Law project (I.C.C. and A.T.S.). The LANL designation for this manuscript is LA-UR-26-24734. The work is funded in part by NSF grants 1818914, 2325080 (with a subcontract to NC State University from Duke University), 2120757 (with a subcontract to NC State University from the University of Maryland) (HPP and HZ). We acknowledge the computing resources provided by North Carolina State University High Performance Computing Services Core Facility (RRID:SCR_022168).

Appendix A: Magic state cultivation

MSC’s procedure [29] consists of three stages: injection, cultivation, and escape. For the injection stage, one can use any state injection method to prepare a noisy magic state. For the cultivation stage, the core idea is to check the quality of the magic state $|m\rangle_L$ via a phase kickback measurement (the circuit shown in Fig. 10). At the beginning of MSC, a noisy magic state and a GHZ is prepared. One can implement a transversal control unitary gate CU on the GHZ state (control qubits) and magic state (target qubits). The corresponding unitary should be a transversal gate for the cultivated code and satisfies

$$U|m\rangle_L = (+1)|m\rangle_L. \quad (\text{A1})$$

Hence, the GHZ state remains invariant if no errors occur. On the other hand, if errors occur, the GHZ state can be corrupted to other states. Thus, one directly measures each qubit of the GHZ state in the X basis and checks the corresponding parity. If any odd parity results are given, it indicates that an error has occurred. Alternatively, one can also unentangle the GHZ state into a product state in the Z basis and measure each qubit. If measurements give a non-zero outcome, this also means that an error happened. Hence, one discards the entire shot and repeats the process until success.

Since magic states, $T|+\rangle_L$, are commonly investigated, U is usually chosen to be $H_{XY} = \frac{X+Y}{2}$ so that one can check $T|+\rangle_L$ ’s quality. The chosen cultivated code must support a transversal or fold transversal H_{XY} gate. The self-dual quantum CSS code family is a good candidate for $T|+\rangle_L$ cultivation. The fold transversal H_{XY} gate is used on the unrotated surface code and composed of the transversal X gate and fold transversal S gate. With the sequence of operators, SX , the magic state becomes

$$SXT|+\rangle_L = e^{i\frac{\pi}{4}}T|+\rangle_L, \quad (\text{A2})$$

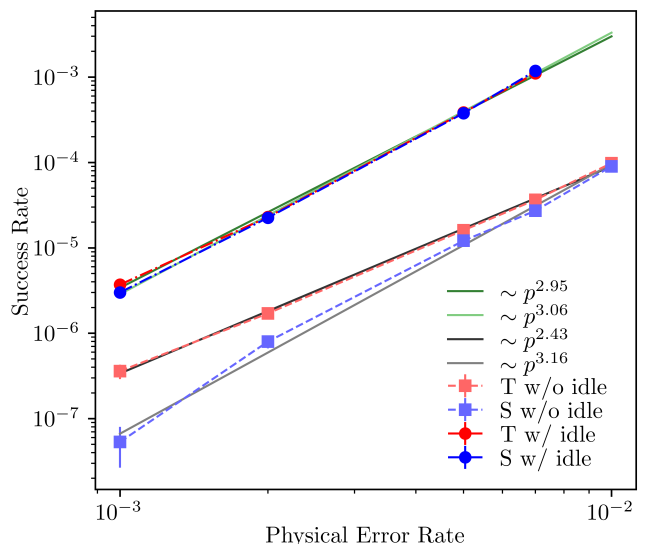


FIG. 11. **Logical infidelities of magic state cultivation.** The logical infidelities of T gate and S gate MSC are estimated under a uniform noise model with (w/ idle), without (w/o idle) ideal noise, and with varied noise levels. The exponents from the fitting lines are calculated using `Scipy.state.linregress` function. Error bars correspond to the standard error of the mean.

which subsequently generates a phase on the GHZ state. One can apply T^\dagger to cancel this phase after disentangling the GHZ state. Beyond H_{XY} checks, only the $U = CX$ are investigated for the magic state $|CX\rangle_L \equiv \frac{|0,+\rangle_L + |0,-\rangle_L + |1,+\rangle_L}{\sqrt{3}}$ [53], which is the resource state for the logical Toffoli implementation [54].

After the phase kickback measurement, known as the cultivation stage [29], the cultivated code must be expanded into the large code so that the high-fidelity state is not significantly affected by memory noise with quantum error correction. For the cultivated 2D color code, one can expand it to the surface code using grafting or LS, which we discussed in the main text. For the rotated surface code, one can expand it using unitary growth, LS, or Li’s protocol [55]. After the escape stage, one can use a complementary gap calculated from the decoder or other soft postselection methods based on the syndrome measurement outcomes to filter out some logical-error-prone results.

According to Ref. [29], $S|+\rangle_L$ and $T|+\rangle_L$ MSC on the $d = 3$ 2D color code give different performance. Moreover, as the noise scale decreases, the difference between the two MSC logical errors becomes larger. Here, to further understand the scaling of 2D color code MSC for $S|+\rangle_L$ and $T|+\rangle_L$, we test their performance under two different noise models, uniform noise models with and without idling, with varying noise levels. We implement MSC followed by 3 rounds of noisy syndrome measurement, a round of ideal syndrome measurements, and an ideal inverse logical T gate or S gate. We then estimate

the logical infidelity using the revival rate from the result, and also discard any shots with syndrome errors.

As Fig. 11 shows, the logical infidelity discrepancy between $T|+\rangle_L$ and $S|+\rangle_L$ becomes larger as the noise level decays. Especially without idling noise, the gap is more significant. At noise level $p = 10^{-3}$, the logical error rate of $T|+\rangle_L$ is roughly 6 times as that of $S|+\rangle_L$. The result shows that the assumption of a factor of 2 difference between $T|+\rangle_L$ and $S|+\rangle_L$ doesn't always hold. Moreover, the scalings of $T|+\rangle_L$ and $S|+\rangle_L$ MSC logical infidelity varying with physical noise level are distinct. Especially, with the uniform noise model without idling noise, the fitting exponent of $S|+\rangle_L$ MSC is 3.16 while that of $T|+\rangle_L$ MSC is 2.42.

Based on this result, it is necessary to have further numerical evidence or analytical calculation for magic cultivation on the 2D color code under different noise models and with $d = 5$ as well. Moreover, it also suggests that other MSCs on the surface code [32, 33, 53, 56] may require more numerical simulation or analytical calculation to verify their $T|+\rangle_L$ MSC result, especially for $d = 5$ MSC. Although Ref. [34] demonstrates ungrown $T|+\rangle_L$ MSC with $d = 5$ and shows its logical error rate are roughly as 8 times as that of $S|+\rangle_L$ MSC, it still requires more samples of simulation to ensure the scaling of $T|+\rangle_L$ MSC and the logical error difference between $S|+\rangle_L$ and $T|+\rangle_L$ MSCs due to the large statistical uncertainty in the numerical result. Moreover, the discrepancy between $T|+\rangle_L$ and $S|+\rangle_L$ MSC behaves differently under different noise models such as for models without idling noise, which are common in ion trap and neutral atom system.

Appendix B: Approximate Noisy Circuit

In our case, Z stabilizer measurement requires 20 ancillary qubits. With data qubits in the $[[15,1,3]]$ code, the entire circuit simulation for the transversal T gate requires 35 qubits, which is difficult to simulate using the state vector simulator. Thus, to tackle this problem, we implement each Z stabilizer measurement individually with a Bell pair and locally apply depolarizing noise to the qubits involved in the stabilizer measurements. For the X stabilizers, we implement the same strategy.

We note that the performance of this approximate circuit differs from that of the original circuit with 35 physical qubits in total. In particular, in the approximate noisy circuit, the accumulated idle noise from each individual stabilizer measurement induces an amount of logical noise. On the other hand, without idle noise, the logical error is not affected by the circuit depth. As Fig. 1 shows, the result of Clifford simulation is consistent with that of state vector simulation for both $T|+\rangle_L$ and $S|+\rangle_L$ preparation.

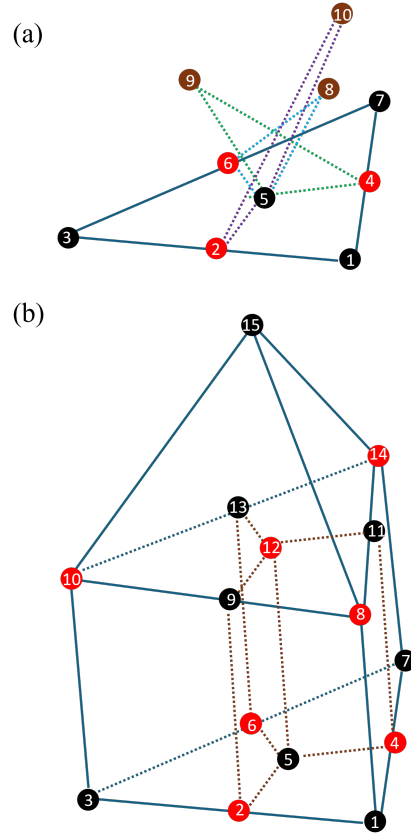


FIG. 12. **The visualization of Vasmer-Kubica code and the 3D $[[15,1,3]]$ color code.** (a) $[[10,1,2]]$ Vasmer-Kubica code. (b) $[[15,1,3]]$ 3D color code (also known as quantum Reed-Muller code). To implement a transversal T gate on a 3D color code, one can simultaneously apply T^\dagger gates on all of the black qubits and T gates on all of the red qubits. On the other hand, for the transversal T gate on the Vasmer-Kubica code, one also applies T^\dagger gates on all of the black qubits, T gates on all of the red qubits, and a CCZ gate on the brown qubits.

Appendix C: Space time volume evaluation

Here, we provide more details on spacetime volume estimation for the magic state preparation methods that we discuss above. Each protocol above can be decomposed into different components. We optimize the quantum circuits for the magic state preparation and estimate the corresponding individual component's spacetime volume.

In Table III, detailed spacetime volume estimates for magic state preparation are shown. For the initialization of the $|+\rangle_L$ on $[[15,1,3]]$ code, without the flag qubit's check, the circuit depth is 5. Since we use 2 4-qubit GHZ states to check the logical state, we can partially parallelize the GHZ state preparation and the $[[15,1,3]]|+\rangle_L$ preparation. Similarly, we also use a Bell pair to check the Steane code's preparation. Thus, we also partially parallelize preparation of Bell pair and $|0\rangle_L$ on $[[7,1,3]]$

Process	Spacetime Volume	Description
$[[15, 1, 3]] +\rangle_L$ preparation	$23 \times 8 + 15 \times 2$	2 4-qubit GHZ states for checking $ +\rangle_L$
$[[7, 1, 3]] 0\rangle_L$ preparation	$7 \times 2 + 9 \times 6$	2 ancilla qubita for checking $ 0\rangle_L$
Z type Stabilizers measurements	35×8	10 Bell states for Z-type syndrome extraction
X type Stabilizers measurements	23×8	4 Bell states for X-type syndrome extraction (only for protocols 1 & 2)
15q GHZ double phase kickback check	11×13 (13×30)	To check $[[15, 1, 3]]$ magic state (only for protocols 1 & 2)
Transversal T	15	Apply T and T^\dagger on each physical qubit of $[[15, 1, 3]]$ code
Logical X measurement on $[[15, 1, 3]]$	15	Measure each physical qubit in X basis
Transversal CNOT	22	Transversal CNOT between Steane code and doubled color code
2D Lattice Surgery ($d_i = 3$ to $d_f = 11$)	$255 \times 21 + 241 \times 6$	3 rounds of surface code syndrome measurement
3D Lattice Surgery ($d_i = 3$ to $d_f = 11$)	$277 \times 24 + 241 \times 6$	3 rounds of surface code syndrome measurement
10 rounds of syndrome measurement	$241 \times 6 \times 10$	Waiting for complementary gap calculation

TABLE III. **The spacetime volume of different parts of magic state preparation**. For the double phase kickback check, protocol 1 doesn't need layers of phase gate to cancel the phase. The corresponding spacetime volume is 11×30 . In contrast, protocol 2 needs layers of T and T^\dagger gates to cancel the extra phase. Hence, the total space time volume is 13×30 . Additionally, transversal CNOT is only used for the 2D LS.

code. To optimize the parallelization, we also use Bell pairs to extract the syndrome for Z and X stabilizers. Only protocols 1 and 2 involve the GHZ double phase kickback check and X stabilizer measurement. Therefore, the total spacetime volumes of protocols 1 and 2 are larger than those without the double phase kickback check. During LS, we implement the Z or X color code stabilizer measurements to parallelize the surface code syndrome measurement cycle. Since X or Z syndrome measurements in 2D (doubled) color code require one (two, resp.) more circuit depth than surface code cycle, the total circuit depth for each round of LS is 7 (8) instead of 6. After the final measurement of the color code, a single round of surface code stabilizer measurement is applied to stabilizers at the boundary of the surface code. In total, for $d = 3$, there are 3 rounds of LS. However, for the color code, there are only two rounds of stabilizer measurement (including the final measurement of all qubits of the color code in X basis). After LS, we also implement an extra 10 rounds of syndrome measurement on the surface code in order to wait for the calculation from the decoder for complementary gap based postselection. The main contribution of the spacetime volume comes from these 10 extra rounds of stabilizer measurements.

To calculate the expected spacetime volume per successful shot (V in eq. 3.1), we also obtain the success rate for different parts of the circuit from the protocols we mentioned. Although protocols 1 and 2 give different success rates at the end, as Table II shows, they provide similar V to achieve an infidelity 1.5×10^{-5} for the magic state.

Appendix D: Doubled color code and Vasmer-Kubica code

The 3D color code $[[15, 1, 3]]$ is also known as the Quantum Reed-Muller (QRM) code. It can be obtained by the doubling the construction from the $[[7, 1, 3]]$ Steane code with fixed gauges. It has 4 8-weight X stabilizers and 10 4-weight Z stabilizers, which are on the cells and the faces, respectively, as seen in Fig. 12(b). The corresponding X checks are

$$S_{X,[[15,1,3]]} = \begin{pmatrix} X_1 X_2 X_4 X_5 X_8 X_9 X_{11} X_{12} \\ X_2 X_3 X_5 X_6 X_9 X_{10} X_{12} X_{13} \\ X_4 X_5 X_6 X_7 X_{11} X_{12} X_{13} X_{14} \\ X_8 X_9 X_{10} X_{11} X_{12} X_{13} X_{14} X_{15} \end{pmatrix} \quad (D1)$$

and the Z checks are

$$S_{Z,[[15,1,3]]} = \begin{pmatrix} Z_1 Z_2 Z_4 Z_5 \\ Z_2 Z_3 Z_5 Z_6 \\ Z_4 Z_5 Z_6 Z_7 \\ Z_8 Z_9 Z_{11} Z_{12} \\ Z_9 Z_{10} Z_{12} Z_{13} \\ Z_{11} Z_{12} Z_{13} Z_{14} \\ Z_{10} Z_{13} Z_{14} Z_{15} \\ Z_3 Z_6 Z_{10} Z_{13} \\ Z_2 Z_3 Z_9 Z_{10} \\ Z_1 Z_2 Z_8 Z_9 \end{pmatrix} \quad (D2)$$

The Z logical operators exist on the edge of the tetrahedron. Hence, the corresponding code distance for Z errors is $d_z = 3$. On the other hand, the X stabilizers are located at the face of the tetrahedron. The code distance for X errors is $d_x = 7$.

The Vasmer-Kubica code is a $[[10, 1, 2]]$ code morphed from the $[[15, 1, 3]]$ quantum Reed-Muller code with a subset of qubits that defines $[[8, 3, 2]]$ code [39]. It has 3

	Z	X
[[49, 1, 5]]	$Z_2 Z_3 Z_5 Z_6$	$\left(\begin{array}{c} X_1 X_2 X_3 X_4 X_5 X_6 X_7 X_8 \\ X_2 X_3 X_5 X_6 X_9 X_{10} X_{12} X_{14} \\ X_3 X_4 X_6 X_7 X_{10} X_{11} X_{14} X_{13} \\ X_5 X_6 X_7 X_8 X_{11} X_{14} X_{13} X_{15} \\ S_{24} \\ X_{16} X_{17} X_{18} X_{19} X_{33} X_{34} X_{35} X_{36} \\ X_{17} X_{19} X_{22} X_{23} X_{34} X_{36} X_{39} X_{40} \\ X_{22} X_{23} X_{26} X_{27} X_{39} X_{40} X_{43} X_{44} \\ X_{26} X_{27} X_{31} X_{32} X_{43} X_{44} X_{48} X_{49} \\ X_{18} X_{19} X_{21} X_{26} X_{31} X_{30} X_{25} X_{21} X_{35} X_{36} X_{39} X_{43} X_{48} X_{47} X_{42} X_{38} \\ X_{20} X_{21} X_{24} X_{25} X_{37} X_{38} X_{41} X_{42} \\ X_{24} X_{25} X_{29} X_{30} X_{41} X_{42} X_{46} X_{47} \\ X_{20} X_{24} X_{28} X_{29} X_{37} X_{41} X_{45} X_{46} \end{array} \right)$
	$Z_3 Z_4 Z_6 Z_7$	
	$Z_5 Z_6 Z_7 Z_8$	
	$Z_9 Z_{10} Z_{12} Z_{14}$	
	$Z_{10} Z_{11} Z_{13} Z_{14}$	
	$Z_{11} Z_{12} Z_{13} Z_{14}$	
	$Z_1 Z_2 Z_5 Z_8$	
	$Z_2 Z_5 Z_9 Z_{12}$	
	$Z_2 Z_3 Z_9 Z_{10}$	
	$Z_3 Z_4 Z_{10} Z_{11}$	
	$Z_{16} Z_{17} Z_{18} Z_{19}$	
	$Z_{33} Z_{34} Z_{35} Z_{36}$	
	$Z_{17} Z_{19} Z_{22} Z_{23}$	
	$Z_{34} Z_{36} Z_{39} Z_{40}$	
	$Z_{22} Z_{23} Z_{26} Z_{27}$	
	$Z_{39} Z_{40} Z_{43} Z_{44}$	
	$Z_{26} Z_{27} Z_{31} Z_{32}$	
	$Z_{43} Z_{44} Z_{48} Z_{49}$	
	$Z_{18} Z_{19} Z_{22} Z_{26} Z_{31} Z_{30} Z_{25} Z_{21}$	
	$Z_{35} Z_{36} Z_{39} Z_{43} Z_{48} Z_{47} Z_{42} Z_{38}$	
	$Z_{20} Z_{21} Z_{24} Z_{25}$	
	$Z_{37} Z_{38} Z_{41} Z_{42}$	
	$Z_{24} Z_{25} Z_{29} Z_{30}$	
	$Z_{41} Z_{42} Z_{46} Z_{47}$	
	$Z_{20} Z_{24} Z_{28} Z_{29}$	
	$Z_{37} Z_{41} Z_{45} Z_{46}$	
	$Z_9 Z_{12} Z_{15} Z_{28} Z_{29} Z_{30} Z_{31} Z_{32}$	
	$Z_{20} Z_{21} Z_{37} Z_{38}$	
	$Z_{20} Z_{28} Z_{37} Z_{45}$	
	$Z_{18} Z_{19} Z_{35} Z_{36}$	
	$Z_{19} Z_{22} Z_{36} Z_{39}$	
	$Z_{22} Z_{26} Z_{39} Z_{43}$	
	$Z_{26} Z_{31} Z_{43} Z_{48}$	
	$Z_{31} Z_{32} Z_{48} Z_{49}$	
$Z_{28} Z_{29} Z_{45} Z_{46}$		

TABLE IV. **The stabilizers of [[49, 1, 5]].** $S_{24} = X_9 X_{10} X_{11} X_{12} X_{14} X_{13} X_{15} X_{16} X_{17} X_{18} X_{19} X_{20} X_{21} X_{22} X_{23} X_{24} X_{25} X_{26} X_{27} X_{28} X_{29} X_{30} X_{31} X_{32}$ The labels correspond to the label in Fig. 13 (b).

3-weight Z stabilizers and 3 4-weight Z stabilizers. As Fig. 12(a) shows, The corresponding Z checks are given by

$$S_{Z,[[10,1,2]]} = \begin{pmatrix} Z_1 Z_2 Z_4 Z_5 \\ Z_2 Z_3 Z_5 Z_6 \\ Z_4 Z_5 Z_6 Z_7 \\ Z_2 Z_5 Z_{10} \\ Z_4 Z_5 Z_9 \\ Z_5 Z_6 Z_8 \end{pmatrix}. \quad (\text{D3})$$

There are 3 5-weight X stabilizers for the Vasmer-

Kubica code

$$S_{X,[[10,1,2]]} = \begin{pmatrix} X_1 X_2 X_4 X_5 X_8 \\ X_2 X_3 X_5 X_6 X_9 \\ X_4 X_5 X_6 X_7 X_{10} \end{pmatrix}. \quad (4.4)$$

The code also has Z logical operators $Z_1 Z_8, Z_3 Z_9, Z_7 Z_{10}$. Hence, its Z code distance is 2. On the the other hand, there is the X logical operator $X_1 X_2 X_3 X_4 X_5 X_6 X_7$. The code distance for X error is 7. In Fig. 12(a), we see that the code supports transversal T by applying physical T gates on the black qubits, T^\dagger gates on the red qubits, and a CCZ gate on the brown qubits.

When $d = 5$, one can construct the $d = 5$ dou-

	Z	X
[[53, 1, 5]]	$Z_2 Z_3 Z_5 Z_6$	$\left(\begin{array}{c} X_1 X_2 X_3 X_4 X_5 X_6 X_7 X_8 \\ X_2 X_3 X_5 X_6 X_9 X_{10} X_{12} X_{14} \\ X_3 X_4 X_6 X_7 X_{10} X_{11} X_{14} X_{13} \\ X_5 X_6 X_7 X_8 X_{11} X_{14} X_{13} X_{15} \\ S_{26} \\ X_{16} X_{17} X_{25} X_{21} X_{35} X_{36} X_{44} X_{40} \\ X_{17} X_{18} X_{21} X_{22} X_{36} X_{37} X_{40} X_{41} \\ X_{18} X_{19} X_{23} X_{27} X_{26} X_{22} X_{37} X_{38} X_{42} X_{46} X_{45} X_{41} \\ X_{19} X_{20} X_{23} X_{24} X_{38} X_{39} X_{42} X_{43} \\ X_{21} X_{22} X_{26} X_{29} X_{28} X_{25} X_{40} X_{41} X_{45} X_{48} X_{47} X_{44} \\ X_{23} X_{24} X_{30} X_{27} X_{42} X_{43} X_{49} X_{46} \\ X_{31} X_{32} X_{30} X_{27} X_{26} X_{29} \\ X_{31} X_{32} X_{30} X_{27} X_{26} X_{29} \\ X_{50} X_{51} X_{49} X_{46} X_{45} X_{48} \\ X_{22} X_{26} X_{30} X_{31} \\ X_{32} X_{31} X_{28} X_{29} \\ X_{34} X_{32} X_{31} X_{33} \\ X_{53} X_{52} X_{50} X_{51} \\ X_9 Z_{10} Z_{11} Z_{16} Z_{17} Z_{18} Z_{19} Z_{20} \\ Z_{19} Z_{20} Z_{38} Z_{39} \\ Z_{16} Z_{17} Z_{35} Z_{36} \\ Z_{16} Z_{25} Z_{35} Z_{44} \\ Z_{21} Z_{22} Z_{40} Z_{41} \\ Z_{22} Z_{36} Z_{41} Z_{45} \\ Z_{26} Z_{27} Z_{45} Z_{46} \\ Z_{29} Z_{26} Z_{45} Z_{48} \\ Z_{29} Z_{31} Z_{48} Z_{50} \\ Z_{23} Z_{27} Z_{42} Z_{46} \end{array} \right)$
	$Z_3 Z_4 Z_6 Z_7$	
	$Z_5 Z_6 Z_7 Z_8$	
	$Z_9 Z_{10} Z_{12} Z_{14}$	
	$Z_{10} Z_{11} Z_{13} Z_{14}$	
	$Z_{11} Z_{12} Z_{13} Z_{14}$	
	$Z_1 Z_2 Z_5 Z_8$	
	$Z_2 Z_5 Z_9 Z_{12}$	
	$Z_2 Z_3 Z_9 Z_{10}$	
	$Z_3 Z_4 Z_{10} Z_{11}$	
	$Z_{16} Z_{17} Z_{25} Z_{21}$	
	$Z_{35} Z_{36} Z_{44} Z_{40}$	
	$Z_{17} Z_{18} Z_{21} Z_{22}$	
	$Z_{36} Z_{37} Z_{40} Z_{41}$	
	$Z_{18} Z_{19} Z_{23} Z_{27} Z_{26} Z_{22}$	
	$Z_{37} Z_{38} Z_{42} Z_{46} Z_{45} Z_{41}$	
	$Z_{19} Z_{20} Z_{23} Z_{24}$	
	$Z_{38} Z_{39} Z_{42} Z_{43}$	
	$Z_{21} Z_{22} Z_{26} Z_{29} Z_{28} Z_{25}$	
	$Z_{40} Z_{41} Z_{45} Z_{48} Z_{47} Z_{44}$	
	$Z_{23} Z_{24} Z_{30} Z_{27}$	
	$Z_{42} Z_{43} Z_{49} Z_{46}$	
	$Z_{31} Z_{32} Z_{30} Z_{27} Z_{26} Z_{29}$	
	$Z_{50} Z_{51} Z_{49} Z_{46} Z_{45} Z_{48}$	
	$Z_{22} Z_{26} Z_{30} Z_{31}$	
	$Z_{32} Z_{31} Z_{28} Z_{29}$	
	$Z_{34} Z_{32} Z_{31} Z_{33}$	
	$Z_{53} Z_{52} Z_{50} Z_{51}$	
	$Z_9 Z_{10} Z_{11} Z_{16} Z_{17} Z_{18} Z_{19} Z_{20}$	
	$Z_{19} Z_{20} Z_{38} Z_{39}$	
	$Z_{16} Z_{17} Z_{35} Z_{36}$	
	$Z_{16} Z_{25} Z_{35} Z_{44}$	
	$Z_{21} Z_{22} Z_{40} Z_{41}$	
	$Z_{22} Z_{36} Z_{41} Z_{45}$	
	$Z_{26} Z_{27} Z_{45} Z_{46}$	
$Z_{29} Z_{26} Z_{45} Z_{48}$		
$Z_{29} Z_{31} Z_{48} Z_{50}$		
$Z_{23} Z_{27} Z_{42} Z_{46}$		

TABLE V. **The stabilizers of** $[[53, 1, 5]]$. $S_{26} = X_9 X_{10} X_{11} X_{12} X_{14} X_{13} X_{15} X_{16} X_{17} X_{18} X_{19} X_{20} X_{21} X_{22} X_{23} X_{24} X_{25} X_{26} X_{27} X_{28} X_{29} X_{30} X_{31} X_{32} X_{33} X_{34}$ is a 26-weight stabilizer. The labels correspond to the label in Fig. 13 (a).

bled code using double construction. Based on the double construction protocol, one needs a $d = 3$ tri-orthogonal code $[[n_{tri}, 1, 3]]$ and $d = 5$ quantum with code parameters $[[n_{sd}, 1, 5]]$ to construct the doubled code $[[n_{tri} + 2n_{sd}, 1, 5]]$. For the tri-orthogonal code, we select the QRM code $[[15, 1, 3]]$ described above. On the other hand, the $d = 5$ 2D color code $[[19, 1, 5]]$ and the $[[17, 1, 5]]$ code can be the self-dual code to construct the doubled color code $[[53, 1, 5]]$ and $[[49, 1, 5]]$ (shown in Fig. 13) respectively. $[[49, 1, 5]]$ has 35 Z stabilizers, which are

located on the faces and given in the table, and X stabilizers, which are on the cells. Since these codes still retain their 2D color code Z stabilizers, the codes still support the CS to $d = 5$ 2D color code using a one way transversal CNOT.

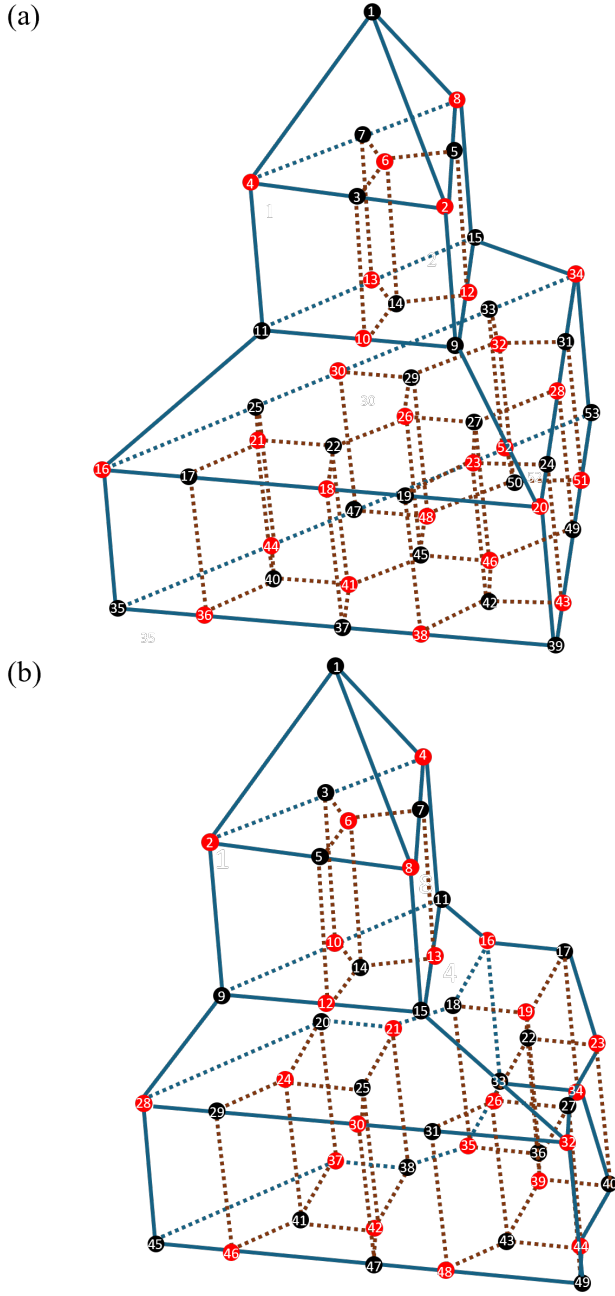


FIG. 13. **The visualization of 3D recursive capped color code.** (a) $[[49,1,5]]$ code constructed from $[[17,1,5]]$ code. (b) $[[53,1,5]]$ code constructed from $[[19,1,5]]$ code. To implement the transversal T gate on those two code, one can apply physical T gates on the black qubits and T^\dagger on the red qubits. The X (Z) type of stabilizers are on the cells (faces).

-
- [1] P. Shor, Fault-tolerant quantum computation, in *Proceedings of 37th Conference on Foundations of Computer Science* (1996) pp. 56–65.
- [2] E. T. Campbell, B. M. Terhal, and C. Vuillot, Roads towards fault-tolerant universal quantum computation, *Nature* **549**, 172 (2017).
- [3] T. J. Yoder, R. Takagi, and I. L. Chuang, Universal fault-tolerant gates on concatenated stabilizer codes, *Phys. Rev. X* **6**, 031039 (2016).
- [4] B. Eastin and E. Knill, Restrictions on transversal encoded quantum gate sets, *Phys. Rev. Lett.* **102**, 110502 (2009).
- [5] D. Horsman, A. G. Fowler, S. Devitt, and R. V. Meter, Surface code quantum computing by lattice surgery, *New Journal of Physics* **14**, 123011 (2012).
- [6] D. Litinski, A Game of Surface Codes: Large-Scale Quantum Computing with Lattice Surgery, *Quantum* **3**, 128 (2019).
- [7] M. A. Nielsen and I. L. Chuang, *Quantum Computation and Quantum Information: 10th Anniversary Edition* (Cambridge University Press, 2010).
- [8] H. Bombín, Dimensional jump in quantum error correction, *New Journal of Physics* **18**, 043038 (2016).
- [9] J. Dehaene and B. De Moor, Clifford group, stabilizer states, and linear and quadratic operations over $\text{gf}(2)$, *Phys. Rev. A* **68**, 042318 (2003).
- [10] C. Chamberland, A. Kubica, T. J. Yoder, and G. Zhu, Triangular color codes on trivalent graphs with flag qubits, *New Journal of Physics* **22**, 023019 (2020).
- [11] A. Wu, K. Yin, A. W. Cross, A. Li, and Y. Ding, Enabling Full-Stack Quantum Computing with Changeable Error-Corrected Qubits, arXiv [10.48550/arXiv.2305.07072](https://arxiv.org/abs/10.48550/arXiv.2305.07072) (2023).
- [12] H. Bombin and M. A. Martin-Delgado, Topological computation without braiding, *Phys. Rev. Lett.* **98**, 160502 (2007).
- [13] A. Kubica and M. E. Beverland, Universal transversal gates with color codes: A simplified approach, *Phys. Rev. A* **91**, 032330 (2015).
- [14] J. T. Anderson, G. Duclos-Cianci, and D. Poulin, Fault-tolerant conversion between the steane and reed-muller quantum codes, *Phys. Rev. Lett.* **113**, 080501 (2014).
- [15] H. Bombín, Gauge color codes: optimal transversal gates and gauge fixing in topological stabilizer codes, *New Journal of Physics* **17**, 083002 (2015).
- [16] F. Butt, S. Heußen, M. Rispler, and M. Müller, Fault-tolerant code-switching protocols for near-term quantum processors, *PRX Quantum* **5**, 020345 (2024).
- [17] S. Heußen and J. Hilder, Efficient fault-tolerant code switching via one-way transversal CNOT gates, *Quantum* **9**, 1846 (2025).
- [18] I. Pogorelov, F. Butt, L. Postler, C. D. Marciniak, P. Schindler, M. Müller, and T. Monz, Experimental fault-tolerant code switching, *Nature Physics* **21**, 298 (2025).
- [19] S. Bravyi, M. Suchara, and A. Vargo, Efficient algorithms for maximum likelihood decoding in the surface code, *Phys. Rev. A* **90**, 032326 (2014).
- [20] L. Aghababaie Beni, O. Higgott, and N. Shutty, *Tesseract: A search-based decoder for quantum error correction* (2025), arXiv:2503.10988 [quant-ph].
- [21] S. Koutsoumpas, T. Noszko, H. Sayginel, M. Webster, and J. Roffe, Colour Codes Reach Surface Code Performance using Vibe Decoding, arXiv [10.48550/arXiv.2508.15743](https://arxiv.org/abs/10.48550/arXiv.2508.15743) (2025).
- [22] O. Higgott and C. Gidney, Sparse Blossom: correcting a million errors per core second with minimum-weight matching, *Quantum* **9**, 1600 (2025).
- [23] L. Daguerre, R. Blume-Kohout, N. C. Brown, D. Hayes, and I. H. Kim, Experimental demonstration of high-fidelity logical magic states from code switching, *Phys. Rev. X* **15**, 041008 (2025).
- [24] L. Daguerre and I. H. Kim, Code switching revisited: Low-overhead magic state preparation using color codes, *Phys. Rev. Res.* **7**, 023080 (2025).
- [25] F. Butt, L. Esser, and M. Müller, Decoding 3d color codes with boundaries, arXiv [10.48550/arXiv.2512.13436](https://arxiv.org/abs/10.48550/arXiv.2512.13436) (2025).
- [26] S. Bravyi and A. Kitaev, Universal quantum computation with ideal clifford gates and noisy ancillas, *Phys. Rev. A* **71**, 022316 (2005).
- [27] S. Bravyi and J. Haah, Magic-state distillation with low overhead, *Phys. Rev. A* **86**, 052329 (2012).
- [28] J. Haah and M. B. Hastings, Codes and Protocols for Distilling T , controlled- S , and Toffoli Gates, *Quantum* **2**, 71 (2018).
- [29] C. Gidney, N. Shutty, and C. Jones, Magic state cultivation: growing T states as cheap as CNOT gates, arXiv [10.48550/arXiv.2409.17595](https://arxiv.org/abs/10.48550/arXiv.2409.17595) (2024).
- [30] E. Rosenfeld, C. Gidney, G. Roberts, A. Morvan, N. Lacroix, D. Kafri, J. Marshall, M. Li, V. Sivak, D. Abanin, A. Abbas, R. Acharya, L. A. Beni, G. Aigeldinger, R. Alcaraz, S. Alcaraz, T. I. Andersen, M. Ansmann, F. Arute, K. Arya, W. Askew, N. Astrakhantsev, J. Atalaya, R. Babbush, B. Ballard, J. C. Bardin, H. Bates, A. Bengtsson, M. B. Karimi, A. Bilmes, S. Bilodeau, F. Borjans, J. Bovaird, D. Bowers, L. Brill, P. Brooks, M. Broughton, D. A. Browne, B. Buchea, B. B. Buckley, T. Burger, B. Burkett, N. Bushnell, J. Busnaina, A. Cabrera, J. Campero, H.-S. Chang, S. Chen, Z. Chen, B. Chiaro, L.-Y. Chih, A. Y. Cleland, B. Cochrane, M. Cockrell, J. Cogan, P. Conner, H. Cook, R. G. Cortiñas, W. Courtney, A. L. Crook, B. Curtin, M. Damyanov, S. Das, D. M. Debroy, S. Demura, P. Donohoe, I. Drozdov, A. Dunsworth, V. Ehimhen, A. Eickbusch, A. M. Elbag, L. Ella, M. Elzouka, D. Enriquez, C. Erickson, L. Faoro, V. S. Ferreira, M. Flores, L. F. Burgos, S. Fontes, E. Forati, J. Ford, B. Foxen, M. Fukami, A. W. L. Fung, L. Fuste, S. Ganjam, G. Garcia, C. Garrick, R. Gasca, H. Gehring, R. Geiger, É. Genois, W. Giang, D. Gilboa, J. E. Goeders, E. C. Gonzales, R. Gosula, S. J. de Graaf, A. G. Dau, D. Graumann, J. Grebel, A. Greene, J. A. Gross, J. Guerrero, L. L. Guevel, T. Ha, S. Habegger, T. Hadick, A. Hadjikhani, M. C. Hamilton, M. Hansen, M. P. Harrigan, S. D. Harrington, J. Hartshorn, S. Heslin, P. Heu, O. Higgott, R. Hiltermann, J. Hilton, H.-Y. Huang, M. Hucka, C. Hudspeth, A. Huff, W. J. Huggins, L. B. Ioffe, E. Jeffrey, S. Jevons, Z. Jiang, X. Jin, C. Joshi, P. Juhas, A. Kabel, H. Kang, K. Kang, A. H. Karamlou, R. Kaufman, K. Kechedzhi, T. Khattar, M. Khezri, S. Kim, P. V. Klimov, C. M. Knaut, B. Kobrin, A. N.

- Korotkov, F. Kostritsa, J. M. Kreikebaum, R. Kudo, B. Kueffler, A. Kumar, V. D. Kurilovich, V. Kutsko, T. Lange-Dei, B. W. Langley, P. Laptev, K.-M. Lau, E. Leavell, J. Ledford, J. Lee, K. Lee, B. J. Lester, W. Leung, L. Li, W. Y. Li, A. T. Lill, W. P. Livingston, M. T. Lloyd, A. Locharla, L. De Lorenzo, E. Lucero, D. Lundahl, A. Lunt, S. Madhuk, A. Maiti, A. Maloney, S. Mandrà, L. S. Martin, O. Martin, E. Mascot, P. M. Das, D. Maslov, M. Mathews, C. Maxfield, J. R. McClean, M. McEwen, S. Meeks, A. Megrant, K. C. Miao, Z. K. Mineev, R. Molavi, S. Molina, S. Montazeri, C. Neill, M. Newman, A. Nguyen, M. Nguyen, C.-H. Ni, M. Y. Niu, N. Noll, L. Oas, W. D. Oliver, R. Orosco, K. Ottosson, A. Pagano, A. Di Paolo, S. Peek, D. Peterson, A. Pizzuto, E. Portoles, R. Potter, O. Pritchard, M. Qian, C. Quintana, G. Ramachandran, A. Ranadive, M. J. Reagor, R. Resnick, D. M. Rhodes, D. Riley, R. Rodriguez, E. Ropes, L. B. De Rose, E. Rosenberg, D. Rosenstock, E. Rossi, P. Roushan, D. A. Rower, R. Salazar, K. Sankaragomathi, M. C. Sarihan, M. Schaefer, S. Schroeder, H. F. Schurkus, A. Shahingohar, M. J. Shearn, A. Shorter, N. Shutty, V. Shvarts, S. Small, W. C. Smith, D. A. Sobel, B. Spells, S. Springer, G. Sterling, J. Suchard, A. Szasz, A. Szein, M. Taylor, J. P. Thiruraman, D. Thor, D. Timucin, E. Tomita, A. Torres, M. M. Torunbalci, H. Tran, A. Vaishnav, J. Vargas, S. Vdovichev, G. Vidal, B. Villalonga, C. V. Heidweiller, M. Voorhees, S. Waltman, J. Waltz, S. X. Wang, D. Wang, B. Ware, J. D. Watson, Y. Wei, T. Weidel, T. White, K. Wong, B. W. K. Woo, C. J. Wood, M. Woodson, C. Xing, Z. J. Yao, P. Yeh, B. Ying, J. Yoo, N. Yosri, E. Young, G. Young, A. Zalcman, R. Zhang, Y. Zhang, N. Zhu, N. Zobrist, Z. Zou, H. Neven, S. Boixo, C. Jones, J. Kelly, A. Bourassa, and K. J. Satzinger, Magic state cultivation on a superconducting quantum processor, arXiv [10.48550/arXiv.2512.13908](https://arxiv.org/abs/10.48550/arXiv.2512.13908) (2025).
- [31] Y. Hirano, R. Toshio, T. Itogawa, and K. Fujii, Efficient magic state cultivation with lattice surgery, arXiv [10.48550/arXiv.2510.24615](https://arxiv.org/abs/10.48550/arXiv.2510.24615) (2025).
- [32] Z.-H. Chen, M.-C. Chen, C.-Y. Lu, and J.-W. Pan, Efficient Magic State Cultivation on $\mathbb{R}P^2$, arXiv [10.48550/arXiv.2503.18657](https://arxiv.org/abs/10.48550/arXiv.2503.18657) (2025).
- [33] K. Sahay, P.-K. Tsai, K. Chang, Q. Su, T. B. Smith, S. Singh, and S. Puri, Fold-transversal surface code cultivation, arXiv [10.48550/arXiv.2509.05212](https://arxiv.org/abs/10.48550/arXiv.2509.05212) (2025).
- [34] R. Li, K. Zheng, Y. Zhang, H. Lou, S. Ying, K. Liu, and X. Sun, Soft: a high-performance simulator for universal fault-tolerant quantum circuits, arXiv [10.48550/arXiv.2512.23037](https://arxiv.org/abs/10.48550/arXiv.2512.23037) (2025).
- [35] B. A. Chase and F. Labib, [CliffT: Fast exact simulation of near-clifford quantum circuits](https://arxiv.org/abs/2604.27058) (2026), arXiv:2604.27058 [quant-ph].
- [36] D. Bluvstein, A. A. Geim, S. H. Li, S. J. Evered, J. P. Bonilla Ataides, G. Baranes, A. Gu, T. Manovitz, M. Xu, M. Kalinowski, S. Majidy, C. Kokail, N. Maskara, E. C. Trapp, L. M. Stewart, S. Hollerith, H. Zhou, M. J. Gullans, S. F. Yelin, M. Greiner, V. Vuletić, M. Cain, and M. D. Lukin, A fault-tolerant neutral-atom architecture for universal quantum computation, *Nature* **649**, 39 (2025).
- [37] R. Wille, L. Berent, T. Forster, J. Kunasaikaran, K. Mato, T. Peham, N. Quetschlich, D. Rovara, A. Sander, L. Schmid, D. Schoenberger, Y. Stade, and L. Burgholzer, The MQT handbook: A summary of design automation tools and software for quantum computing, in *IEEE International Conference on Quantum Software (QSW)* (2024) 2405.17543.
- [38] T. Peham, L. Schmid, L. Berent, M. Müller, and R. Wille, Automated synthesis of fault-tolerant state preparation circuits for quantum error-correction codes, *PRX Quantum* **6**, 020330 (2025).
- [39] M. Vasmer and A. Kubica, Morphing quantum codes, *PRX Quantum* **3**, 030319 (2022).
- [40] Y. Takada and K. Fujii, Improving threshold for fault-tolerant color-code quantum computing by flagged weight optimization, *PRX Quantum* **5**, 030352 (2024).
- [41] S. Bravyi and A. Cross, Doubled Color Codes, arXiv [10.48550/arXiv.1509.03239](https://arxiv.org/abs/1509.03239) (2015).
- [42] S. P. Jain and V. V. Albert, Transversal clifford and t-gate codes of short length and high distance, *IEEE Journal on Selected Areas in Information Theory* **6**, 127 (2025).
- [43] M. Sullivan, Code conversion with the quantum golay code for a universal transversal gate set, *Phys. Rev. A* **109**, 042416 (2024).
- [44] T. Jochym-O'Connor and S. D. Bartlett, Stacked codes: Universal fault-tolerant quantum computation in a two-dimensional layout, *Phys. Rev. A* **93**, 022323 (2016).
- [45] T. Tansuwannont and D. Leung, Achieving fault tolerance on capped color codes with few ancillas, *PRX Quantum* **3**, 030322 (2022).
- [46] D. Forlivesi and D. Amaro, Flag at origin: a modular fault-tolerant preparation for CSS codes, arXiv [10.48550/arXiv.2508.14200](https://arxiv.org/abs/10.48550/arXiv.2508.14200) (2025).
- [47] C. Gidney, M. Newman, and M. McEwen, Benchmarking the Planar Honeycomb Code, *Quantum* **6**, 813 (2022).
- [48] C. Gidney, M. Newman, P. Brooks, and C. Jones, Yoked surface codes, arXiv [10.48550/arXiv.2312.04522](https://arxiv.org/abs/10.48550/arXiv.2312.04522) (2023).
- [49] I.-C. Chen, M. da Silva Fonseca, and A. Sornborger, [Efficient magic state cultivation for \$\sqrt{T}\$ gates](https://arxiv.org/abs/2606.10430) (2026), arXiv:2606.10430 [quant-ph].
- [50] D. Ruiz, J. Guillaud, C. Vuillot, and M. Mirrahimi, Unfolded distillation: very low-cost magic state preparation for biased-noise qubits, arXiv [10.48550/arxiv.2507.12511](https://arxiv.org/abs/10.48550/arxiv.2507.12511) (2025).
- [51] S.-H. Lee, F. Thomsen, N. Fazio, B. J. Brown, and S. D. Bartlett, Low-overhead magic state distillation with color codes, *PRX Quantum* **6**, 030317 (2025).
- [52] Q. Xu, H. Zhou, D. Bluvstein, M. Cain, M. Kalinowski, J. Preskill, M. D. Lukin, and N. Maskara, Batched high-rate logical operations for quantum LDPC codes, arXiv [10.48550/arXiv.2510.06159](https://arxiv.org/abs/10.48550/arXiv.2510.06159) (2025).
- [53] Y. Vakinin, S. Jacoby, A. Grimsmo, and A. Retzker, Efficient Magic State Cultivation on the Surface Code, arXiv [10.48550/arXiv.2502.01743](https://arxiv.org/abs/10.48550/arXiv.2502.01743) (2025).
- [54] E. Dennis, Toward fault-tolerant quantum computation without concatenation, *Phys. Rev. A* **63**, 052314 (2001).
- [55] Y. Li, A magic state's fidelity can be superior to the operations that created it, *New Journal of Physics* **17**, 023037 (2015).
- [56] J. Claes, Cultivating T states on the surface code with only two-qubit gates, arXiv [10.48550/arXiv.2509.05232](https://arxiv.org/abs/10.48550/arXiv.2509.05232) (2025).